

## Solute trapping effects in planar isothermal solidification of dilute binary alloys

Ch. Charach\*

*Center for Energy and Environmental Physics, Jacob Blaustein Institute for Desert Research, Ben Gurion University of the Negev, Sede Boqer Campus, 84990 Israel*

Y. Keizman

*Department of Fluid Dynamics and Heat Transfer, Faculty of Engineering, Tel Aviv University, Ramat Aviv, 69978 Israel*

(Received 2 June 1995; revised manuscript received 13 December 1995)

Transient rapid solidification of dilute binary alloys is addressed in the frame of the continuous growth model, accounting for solute trapping effects. We consider the planar isothermal growth from a melt of some uniform initial composition. The initial solute concentration in the melt is assumed to be below its equilibrium value. An approximate solution of this problem is developed using the mass balance integral method with the boundary-layer-type profiles for solute concentration. This solution is validated by the numerical solution of the original moving boundary problem. The influence of solute trapping effects on the main evolution characteristics of the process is discussed. The transient regime and the long-time asymptotic states are investigated. The physics of the process is clarified using the Baker-Cahn diagrams for a solute concentration at the interface. [S1063-651X(96)01107-5]

PACS number(s): 05.70.Fh, 81.15.Lm, 81.10.Aj

### I. INTRODUCTION

Sharp interface models of solidification have been a subject of intensive research for several decades [1–25]. Such models are stated in terms of the heat and mass transport in the bulk and the boundary conditions at the free boundary, i.e., at the solid-liquid interface. These conditions involve the interfacial mass, momentum, and energy balance equations, along with the response functions, which define the interface temperature and composition. The fluid flow in the liquid and the deformations in the solid are often neglected. Then the interface momentum balance reduces to the mechanical equilibrium incorporating the surface tension, while the long range transport is governed by diffusion. The response functions involve the equilibrium contribution, incorporating the Gibbs-Thompson effect, and the nonequilibrium contribution, induced by the discontinuity of the chemical potentials across a moving boundary. The nonequilibrium effects reflect the kinetics of the attachment of the atoms to a growing solid.

For materials with rough solid-liquid interface (metals and some organic materials) the thermally activated atomic jumps are very fast. Therefore one can assume a local thermodynamic equilibrium at the interface (instantaneous attachment kinetics). This assumption is adequate for velocities that are typically smaller than 0.1–1 m/s [10]. For higher crystal growth rates it is mandatory to account for the departure from equilibrium. Such conditions might occur in the directional solidification with high pulling velocities, in freezing from an undercooled melt, or at regrowth from pulsed laser-induced melting. At very high growth rates the width of the diffusional boundary layer becomes of the order of the interface thickness. At this point the sharp interface

models break down. Such processes might be addressed within the phase-field models [25–32].

For pure substances the models of attachment kinetics via thermally activated atomic jumps were proposed many years ago [33,34]. The linearized version of such models predicts interfacial undercooling to be proportional to the growth rate. This result also follows from the approach based on the linearized irreversible thermodynamics [10,11].

For binary alloys the semimicroscopic models of attachment kinetics have been considered in [12–20]. Each of them defines a kinetic phase diagram, for which both the liquidus and the solidus depend on the growth rate. As pointed out by Baker and Cahn [6,7] the change of the free energy per mole of solidified material has to be negative. This thermodynamic constraint is obeyed by the models in which the chemical potentials of each species decrease upon incorporation into crystal [14–16], as well as by the models in which the chemical potential of the solvent atoms decreases during crystal growth, while that of the solute atoms increases [12,13,17–20]. When the equilibrium partition coefficient  $k^*$  is less than unity, the former models [14–16] imply that the partition coefficient  $k(V)$  decreases with the solidification rate  $V$ . On the other hand, for the latter models [12,13,17–20]  $k(V)$  is an increasing function of  $V$ , so that the solid composition at the interface might exceed its equilibrium value. The increase of the partition coefficient with the solidification rate is termed “solute trapping.” Existence of this phenomenon is supported by substantial experimental evidence [6,13,20]. Following Refs. [18,19] we refer to the kinetic models of solute trapping in materials with a rough solid-liquid interface as some particular versions of the continuous growth model.

Analytical and numerical solutions of tractable problems of crystal growth provide a theoretical framework to study the interfacial kinetics effects. One of the key problems of this sort is the planar growth of a solid germ. It mimics the spherical growth of a solid particle when the curvature ef-

\*Also at Department of Physics, Ben Gurion University of the Negev, Beer Sheva, Israel.

fects are small. A pure substance growth of a solid germ from an undercooled melt has been addressed within the sharp interface models with the linear attachment kinetics. Long-time asymptotic solutions to this problem have been given in [21–25]. For small undercooling levels these long-time solutions exhibit the diffusion-limited growth  $V \sim t^{-1/2}$  (here  $t$  is time). For large undercooling (hypercooling) the growth is controlled by the interfacial kinetics. In this case for  $t \rightarrow \infty$  the temperature profile in the melt is described by a plane wave traveling with a constant velocity. For this solution the width of the boundary layer is equal to  $D_T/V$ . (Here  $D_T$  is the thermal diffusivity of the melt.) The above results are in agreement with the numerical solution for the spherical growth [5]. At the critical level of undercooling, i.e., at the crossover between the diffusion-controlled and the kinetics-limited growth, the sharp interface model yields  $V \sim t^{-1/3}$  for  $t \rightarrow \infty$ . Analysis of this problem beyond the long-time asymptotics has been recently presented in [24]. It has been shown that for the critical undercooling the long-time asymptotic state is established via a long-lived transient. Notice that the phase-field models of the planar growth [25,26] admit for the critical undercooling either  $V \sim t^{-1/3}$  or  $V = \text{const}$  asymptotic states. Which one of them is selected depends on the ratio of the thermal diffusivity to that of the order parameter field.

Among the response functions, which determine the boundary conditions at the interface of a solidifying binary alloy, the growth rate is most accessible to experimental control. Due to this reason the solute trapping effects have been studied so far mainly in the context of directional solidification, where the constant pulling velocity might be fixed by the externally imposed heat fluxes. This velocity, along with the solute concentration far from the interface, determine the temperature and the composition at the phase-change front. Stability of the constant velocity solutions has been addressed first within the frozen temperature approximation [35]. In this approach the Lewis number  $Le$ , defined as the ratio of the mass diffusivity  $D$  to the thermal diffusivity  $D_T$ , is assumed to be equal to zero. More recently it has been shown that the fraction of latent heat, released at the interface due to the velocity perturbations, might significantly affect the dynamics of the phase-change front even if the Lewis number is very small [36,37].

Similar to the growth of pure materials, discussed above, the solidification of binary alloys into an undercooled melt offers another way to inspect the interfacial kinetics. (Typically, for diluted binary alloys large interface velocities can be reached already for undercoolings of only a few degrees.) For this setup the transient growth is controlled by the temperature and the composition in the liquid far from the phase-change front. In general, growth into an undercooled melt involves redistribution of both the impurities and the heat, liberated at the solid-liquid interface. Analysis of such problems is very complicated. In fact, only a few solutions are known even when the local equilibrium at the interface is assumed [10]. For out-of-equilibrium conditions at the interface it is natural to assume, as the first step, the isothermal conditions in the melt. This approximation, which implies  $Le=0$ , is analogous to the frozen temperature assumption used in the studies of the directional solidification. Obviously, this condition might be violated for sufficiently high

velocities, or for small solute concentrations [10]. For such situations the isothermal approximation for the melt might still be adequate if the heat liberated at the interface is rapidly conducted away into some appropriate sink [13,38]. We will return to this issue in the last section of the paper.

For the binary alloys the planar isothermal growth of a solid germ has been addressed in [15] by ignoring the solute trapping effects and diffusion in the solid. It has been assumed that the initial solute concentration in the melt is below its equilibrium value. The initial thickness of the solid germ has been neglected. An approximate solution of this problem has been developed using the mass balance integral method with a linear concentration profile in the boundary layer. In spite of the highly nonlinear nature of the kinetic model used in [15], the long-time asymptotics of the above solution is similar to that found for the pure substance. In particular,  $V \sim t^{-1/3}$  has been obtained at the crossover between the kinetics-controlled and the diffusion-dominated regimes.

The present paper attempts to extend the aforementioned works for a pure substance [23,24] and for the binary alloys [15]. We address the planar isothermal growth of a solid germ accounting for the solute trapping effects. This problem is analyzed in the frame of the continuous growth models both with and without the solute drag effects [12,18,19]. Following Refs. [15,23,24] the initial thickness of the germ is assumed to be negligibly small. The diffusion in the solid is disregarded, and the initial solute concentration in the melt is assumed to be below its equilibrium value.

A sufficiently simple approximate solution describing the germ growth is developed. It is based on the mass balance integral method with the boundary layer-type melt concentration profiles. The results are in agreement with the numerical solution of the original moving boundary problem. We analyze the initial, the transient, and the long-time stages of the process. It is shown that the interface velocity is monotonically decreasing in time and the solution evolves towards the diffusion-limited, or the kinetics-limited asymptotic attractors. The emerging physical picture is clarified using the Baker-Cahn diagram [7]. Evolution of the germ generates on this diagram a trajectory, reflecting the initial and boundary conditions, as well as the specifics of the kinetics model. For each of the kinetic models the corresponding trajectory is along the curve that defines the solid composition versus the melt composition at the interface. We show that when the solid composition is a monotonically increasing function of the melt composition at the interface, the long-time asymptotics is similar to that of Ref. [15]. However, for each version of the continuous growth model there exists some threshold equilibrium liquid composition at the interface, above which the corresponding curves on the Baker-Cahn diagram are no longer monotonic. In this case the long-time asymptotic states differ from those obtained neglecting the solute trapping effects. We also demonstrate that the same initial conditions might yield rather different long-time asymptotic attractors for two alternative versions of the continuous growth model. It is shown that the long-lived transients are present at the crossover from the diffusion-limited to the kinetics-controlled growth both for the monotonic, as well as for the nonmonotonic trajectories.

## II. CONTINUOUS GROWTH SOLUTE TRAPPING MODEL

Following Refs. [18,19] we begin the analysis by summarizing the main results of the continuous growth solute trapping model. It describes the attachment kinetics for solidification of dilute binary alloys with a rough interface. For such alloys the equilibrium phase diagram is given by

$$T = T_0 - m^* c^*(T), \quad c_S^* = k^* c^*, \quad (1)$$

where  $T$  is the temperature,  $T_0$  is the melting point of the pure solvent, and  $c^*(T)$  and  $c_S^*(T)$  are, respectively, the equilibrium molar concentrations of solute in the liquid adjacent to the interface, and that in the solid. It is assumed that the equilibrium partition coefficient  $k^*$  and the slope of the liquidus  $m^*$  are temperature independent. We also assume that  $m^* > 0$ . If the interface is curved the latter diagram has to be modified by the Gibbs-Thompson effect. The out-of-equilibrium values of the liquid and the solid concentrations at the interface are denoted by  $c_L$  and  $c_S = k c_L$ , respectively. In the continuous growth solute trapping model for dilute binary alloys  $c_S$  and  $c_L$  are related by the nonequilibrium partition coefficient  $k(V)$  given by

$$k(V) = \frac{k^* + V/v_D}{1 + V/v_D}. \quad (2)$$

Here  $v_D$  is the characteristic velocity scale of the solute trapping effects. Thus  $k(V)$  varies from  $k^*$  at  $V=0$ , to  $k=1$  as  $V \rightarrow \infty$ , and at  $V=v_D$ ,  $k=k_D = 1/2(1+k^*)$ . The value of  $v_D$  is usually estimated as the ratio of the diffusivity in the liquid  $D$  to the interface width, which is of the order of a few angstroms. For metallic alloys  $v_D$  is typically about 5 m/s. Smith and Aziz [20] have pointed out that such estimates might be insufficient: correlations between  $v_D$  and  $k^*$  have been observed, and the values of  $v_D$  about 36 m/s–38 m/s have been reported for the Al-Sn and Al-In alloys. As emphasized in Ref. [20], Eq. (2) fits the experimental data surprisingly well even at velocities for which one might question the validity of the sharp interface models.

The continuous growth model defines also the slope of the kinetic liquidus as a function of the solidification rate. In the spirit of the semimicroscopic model for a pure substance [33,34] it is postulated that the velocity of the solid-liquid interface  $V$  might be expressed as

$$V(T, c_L, c_S) = v_0 \{1 - \exp[\Delta G_{\text{eff}}(T, c_L, c_S)/RT]\}. \quad (3)$$

Here  $R$  is the universal gas constant,  $v_0$  is some characteristic velocity (of the order of sound velocity for metallic melts), and  $\Delta G_{\text{eff}}$  is the solidification driving force.

One of the versions of the continuous growth model [12,13,18], referred to in the present paper as Model A, assumes that  $\Delta G_{\text{eff}}$  is equal to the change of free energy per mole of solidified material  $\Delta G_{DF}$

$$\Delta G_{\text{eff}} = \Delta G_{DF} = c_S \Delta \mu_B + (1 - c_S) \Delta \mu_A, \quad (4)$$

where  $\Delta \mu_{(A,B)}$  denote the difference between the chemical potentials of solid and liquid for solvent ( $A$ ) and solute ( $B$ ), respectively. For diluted alloys at some given temperature  $T$

$$\Delta \mu_B / RT = \ln(k/k^*), \quad (5a)$$

$$\begin{aligned} \Delta \mu_A / RT &= \ln[(1 - k c_L)(1 - c^*) / (1 - k^* c^*)(1 - c_L)] \\ &\approx c_L(1 - k) - c^*(1 - k^*). \end{aligned} \quad (5b)$$

Consequently,

$$\Delta G_{DF} / RT \approx c_L [1 - k + k \ln(k/k^*)] - c^*(1 - k^*). \quad (6)$$

Combining Eqs. (3) and (6) for  $(\Delta G_{DF} / RT) \ll 1$  one obtains the following expression for  $c_L$  for Model A:

$$c_L = \frac{c^*(1 - k^*) - (V/v_0)}{1 - k + k \ln(k/k^*)}. \quad (7)$$

Equations (1), (2), and (7) define the kinetic-phase diagram, i.e., the temperature of a planar interface and the solute concentrations in the regions of the solid and liquid adjacent to the phase-change front.

Aziz and Kaplan [18] presented a somewhat different version of the continuous growth model. They allowed reduction of the free energy, driving the interface motion, by dissipating some of it in the solute-solvent redistribution across the interface (solute drag effect). In this model, referred to as Model B, the crystallization free energy is

$$\Delta G_{\text{eff}} = c_L \Delta \mu_B + (1 - c_L) \Delta \mu_A. \quad (8)$$

The change of the molar free energy upon solidification,  $\Delta G_{DF}$  splits into the sum of the crystallization free energy,  $\Delta G_{\text{eff}}$  and the so called ‘‘solute drag’’ free energy  $\Delta G_D$

$$\Delta G_{DF} = \Delta G_{\text{eff}} + \Delta G_D, \quad (9)$$

where  $\Delta G_D$  is given by

$$\Delta G_D = (c_L - c_S)(\Delta \mu_A - \Delta \mu_B). \quad (10)$$

From Eqs. (5), (6), and (9) it follows that

$$c_L = \frac{c^*(1 - k^*) - (V/v_0)}{1 - k + \ln(k/k^*)}. \quad (11)$$

The slope of the kinetic liquidus is obtained by combining Eqs. (1) and (11).

## III. ISOTHERMAL SOLIDIFICATION: THE BAKER-CAHN DIAGRAM FOR CONTINUOUS GROWTH SOLUTE TRAPPING MODELS

According to Baker and Cahn [7] for the physically allowed solidification processes the change of the molar free energy has to be negative. Therefore for an isothermal growth possible solid compositions  $c_S$  that can form from a melt of varying interfacial composition  $0 < c_L < c^*$  are represented by an area of the  $c_S$ - $c_L$  plane, enclosed by the curve  $\Delta G_{DF} = 0$ . In the present paper this thermodynamically allowed domain is referred to as the Baker-Cahn diagram. According to Eq. (6) its boundary  $c'_S = c'_S(c'_L)$  is given by

$$c'_L = \frac{c^*(1 - k^*)}{1 - k + k \ln(k/k^*)}, \quad c'_S = k c'_L. \quad (12)$$

Thermodynamics does not restrict  $k$  to be greater than  $k^*$ . Thus, in Eqs. (12),  $k$  is just a parameter in the range  $[0, \infty)$ . Consequently,  $c'_S$  is a double-valued function of  $c'_L$  in the interval  $c^*(1-k^*) \leq c'_L < c^*$ .

The function  $c'_S = c'_S(c'_L)$  is essentially nonmonotonic. It starts from zero at  $c'_L = 0$  with  $k = \infty$ . This curve is growing with a continuously decreasing slope and gradually reaches its maximum at  $k = 1$ . From then on this function decreases and at  $c'_L = c^*$  it approaches the equilibrium value  $c'_S = k^* c^*$ . The function  $c'_S = c'_S(c'_L)$  reaches zero again at  $c'_L = c^*(1-k^*)$ .

On the Baker-Cahn diagram the kinetic models with  $k(V) < k^*$  are represented by curves located below the straight line  $c_S = k^* c_L$ . On the other hand, the models accounting for the solute trapping are given by curves in the domain  $k^* < k < 1$ . Since the sharp interface models are ill defined for  $V \geq v_D$ , we restrict the analysis to the  $k^* \leq k < k_D$ . [Here  $k_D = k(V_D)$ .] For this region Eqs. (7) and (11) imply that  $c^*$  is bounded from above by  $c_{\max}^* = v_D/V_0(1-k^*)$ . At  $c^* = c_{\max}^*$ ,  $c_L = 0$  when  $V = V_{\max} = V_D$ .

Let us consider now the function  $c_S = c_S(c_L)$  for the continuous growth models. As follows from Eqs. (7) and (11)  $c_L$  is a monotonically decreasing function of the solidification rate  $V$ :  $c_L = 0$  at  $V = v_0 c^* (1-k^*)$  and it tends to its equilibrium value  $c^*$  in the limit  $V \rightarrow 0$ . Since  $dc_L/dV < 0$ , the sign of  $dc_S/dc_L$  is determined by that of  $dc_S/dV$ . For Model A one obtains

$$\frac{dc_S}{dV} = \frac{c_S}{1-k+k \ln(k/k^*)} \left[ \frac{(1-k)^2}{k(V+v_D)} - \frac{1}{c_L v_0} \right]. \quad (13)$$

According to Eq. (13) there are the following three possibilities: (a)  $dc_S/dc_L > 0$  for  $0 \leq c_L \leq c^*$ , when  $c^* < k^* v_D/v_0(1-k^*)^2$ . (b)  $dc_S/dc_L > 0$  for  $0 \leq c_L < c^*$ , and  $dc_S/dc_L = 0$  at  $c_L = c^*$ , if  $c^* = k^* v_D/v_0(1-k^*)^2$ . (c)  $c_S = c_S(c_L)$  is nonmonotonic and has one maximum at  $c_L = c_Q < c^*$ , if  $c^* > k^* v_D/v_0(1-k^*)^2$ . At this maximum the solid composition  $c_S$  is above its equilibrium value  $c_S = c^* k^*$ .

For Model B Eq. (11) yields

$$\frac{dc_S}{dV} = \frac{c_S}{1-k+\ln(k/k^*)} \left[ \frac{(1-k)\ln(k/k^*)}{k(V+v_D)} - \frac{1}{c_L v_0} \right]. \quad (14)$$

As follows from Eq. (14)  $dc_S/dc_L > 0$  when  $c_L \rightarrow 0$ , or  $c_L \rightarrow c^*$ . Hence for Model B the function  $c_S = c_S(c_L)$  is either monotonically increasing for  $0 \leq c_L \leq c^*$ , or has an equal number of maxima and minima (with possible saddle points) in the open interval  $0 < c_L < c^*$ . These extrema are reached at the concentrations  $c_L = c_{LQ}$  defined by

$$c_{LQ} = k(V+v_D)/v_0[(1-k)\ln(k/k^*)]. \quad (15)$$

Equation (15) has no real roots for  $c^*$  below some threshold equilibrium concentration  $c_{cr}^*$  and  $c_S = c_S(c_L)$  is a monotonically increasing function at the interval  $0 \leq c_L \leq c^*$ . (The value of  $c_{cr}^*$  can be found numerically). At  $c^* = c_{cr}^*$  there is a saddle point at some value of  $c_L$  in the open interval  $(0, c^*)$ . For  $c^* > c_{cr}^*$  the function  $c_S = c_S(c_L)$  is nonmonotonic. The

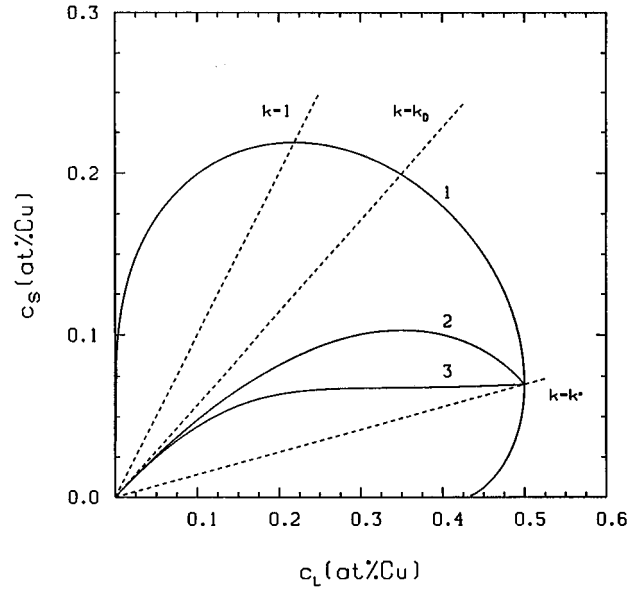


FIG. 1. Baker-Cahn diagram for Al-Cu alloy at  $c^* = 0.5$  at. % Cu. (1) The curve  $\Delta G_{DF} = 0$ , defined by Eq. (12); (2)  $c_S = c_S(c_L)$  for Model A; (3)  $c_S = c_S(c_L)$  for Model B.

numerical studies performed for several metallic alloys have shown that for  $c^* > c_{cr}^*$  there exist one pair of roots of Eq. (15) at  $c_L = c_{LQ1}$  and  $c_L = c_{LQ2} > c_{LQ1}$ , corresponding to the maximum and the minimum, respectively.

In order to illustrate the above considerations we present the results for Al-Cu alloy at  $c^* = 0.5$  at. % Cu. Figure 1 shows the Baker-Cahn diagram. The curve  $c_S = c_S(c_L)$ , corresponding to Model A, has a maximum, whereas that of Model B is increasing monotonically at the entire interval  $0 \leq c_L \leq c^*$ . Figure 2 demonstrates the interface velocity at the extremum points  $V_Q$  as a function of  $c^*$ . For Model A

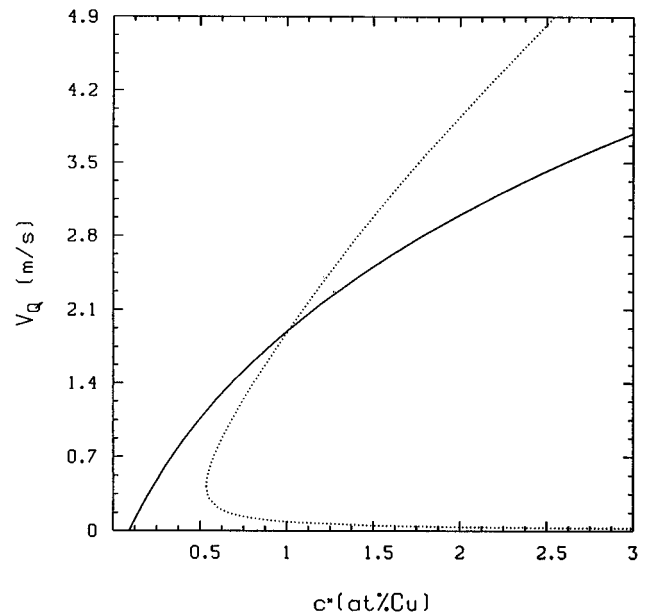


FIG. 2. Interface velocity at the extremum points of  $c_S = c_S(c_L)$ ,  $V_Q$ , as a function of the equilibrium melt composition  $c^*$ . (Al-Cu alloy). Solid line—Model A, dotted line—Model B.

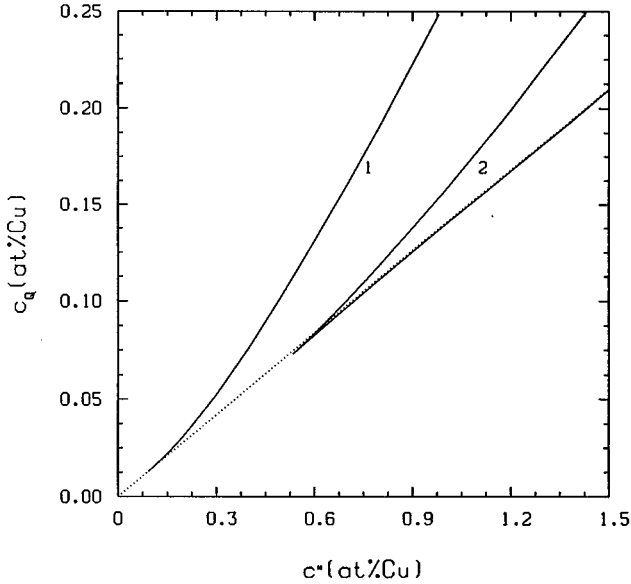


FIG. 3. Solid composition at the extremum points of  $c_S = c_S(c_L)$ ,  $c_{SQ}$  as a function of the equilibrium melt composition  $c^*$  (Al-Cu alloy). Solid line 1—Model A, solid line 2—Model B, dotted line—reference line  $c_S^* = k^* c^*$ .

the solidification rate at the maximal solid composition is increasing with  $c^*$ . For Model B the threshold concentration  $c_{cr}^*$  is about 0.54 at. % Cu. At  $c^* > c_{cr}^*$  the separation between the maximum and the minimum of  $c_S = c_S(c_L)$  increases with  $c^*$ : the minimum point tends to the equilibrium, whereas the maximum point moves in the opposite direction. Figure 3 shows the solid concentration at the extremum points of  $c_S = c_S(c_L)$ , as a function of  $c^*$ . The maximal concentration of  $c_S$ , as given by Model A, is greater than that defined by Model B. Similar results have been obtained for several other metallic alloys.

The above considerations enable one to get a better qualitative understanding of the planar isothermal solidification of dilute binary alloys. Indeed, the composition at the interface at any instant of time might be represented by a point on the curve  $c_S = c_S(c_L)$ , corresponding to some particular model of interfacial kinetics. The advance of the freezing front generates, hereby, a trajectory along this curve. It depends on the boundary and the initial conditions, as well as on the specifics of the kinetics model. In the following sections we will thoroughly discuss the trajectories describing the isothermal growth of a solid germ, and the corresponding long-time asymptotic attractors.

In the present paper it is assumed that the solute concentration at infinity is maintained at a constant value  $c = c_\infty$ . Neglecting the diffusion in the solid, the governing equations for the planar isothermal solidification are stated as follows:

$$\partial c / \partial t = D \partial^2 c / \partial x^2, \quad x > R(t), \quad (16)$$

$$-D(\partial c / \partial x)|_{x=R(t)} = c_L(1-k)V, \quad V = dR/dt, \quad (17)$$

$$c|_{x=R(t)} = c_L, \quad c|_{x=\infty} = c_\infty. \quad (18)$$

Here  $c$  is the solute concentration in the melt,  $R(t)$  is the interface position at time  $t$ , and  $x$  is the spatial coordinate along the direction normal to the solid-liquid interface. The melt composition at the interface is defined by a particular kinetic model. For the continuous growth models it is given by Eq. (7) for Model A, or by Eq. (11) for Model B, respectively. Obviously, Eqs. (16)–(18) have to be supplemented by the initial conditions.

Two particular solutions of the above equations are of special interest. The first one [1,2] assumes a local equilibrium at the interface  $c_L = c^*$ ,  $k = k^*$  and describes the diffusion-controlled growth

$$c = c_\infty + (c^* - c_\infty) \frac{\operatorname{erfc}(\Omega x/R)}{\operatorname{erfc} \Omega}, \quad R(t) = 2\Omega \sqrt{Dt}. \quad (19)$$

Here  $\Omega$  is a root of the transcendental equation

$$\sqrt{\pi} \Omega \exp(\Omega^2) \operatorname{erfc} \Omega = \operatorname{St}, \quad \operatorname{St} = (c^* - c_\infty) / c^* (1 - k^*). \quad (20)$$

Equation (20) admits finite solutions, when the diffusional Stefan number  $\operatorname{St}$  is smaller than unity ( $c_\infty > c^* k^*$ ). For  $\operatorname{St} \rightarrow 1$ , the growth rate diverges, since  $\Omega \rightarrow \infty$ .

Another well known solution [4,7] describes the solidification with a constant interface velocity  $R = Vt$ . The concentration profile in the melt is then given by

$$c = c_\infty + (c_L - c_\infty) \exp[-(V/D)(x - R(t))]. \quad (21)$$

Consistency of this profile with the interfacial mass balance implies

$$c_S = k(V) c_L(V) = c_\infty. \quad (22)$$

Equation (22) determines implicitly the solidification rate  $V$ .

The constant velocity solution represents some point on the curve  $c_S = c_S(c_L)$ . As long as this curve is monotonic for  $0 \leq c_L \leq c^*$ , the maximal value of the solid concentration  $\max\{k c_L\}$  is equal to  $c^* k^*$ , and the plane wave-type solutions are allowed in the range  $0 < c_\infty < c^* k^*$ . In this case for each value of  $c_\infty$  Eq. (22) has only one real root.

For nonmonotonic curves  $c_S = c_S(c_L)$  the constant velocity solutions are permitted for  $0 < c_\infty \leq \max\{k c_L\}$ , and Eq. (22) has multiple roots. For such curves  $\max\{k c_L\}$  depends on the nature of the kinetics model:  $\max\{k c_L\}$  is equal to  $k_Q c_{LQ}$  for Model A, and to the largest among  $k_{Q1} c_{LQ1}$  and  $k^* c^*$  for Model B. As pointed out in [7] the traveling wave-type solutions might be diffusionally unstable for  $c_\infty > c^* k^*$ . The stability of the constant velocity solutions with respect to the planar perturbations has been reconsidered recently [39]. The preliminary analysis indicates that the Baker-Cahn instability, mentioned above, occurs only for those roots of Eq. (22), which are located on the decreasing branch of the  $c_S = c_S(c_L)$  curve. A comprehensive analysis of this issue will be presented in a separate paper.

#### IV. ISOTHERMAL GROWTH OF A SOLID GERM: MASS BALANCE INTEGRAL METHOD

Let us consider now the planar isothermal growth of a solid germ from a melt with the uniform initial concentration

$c_\infty < c^*$ . This problem is described by Eqs. (16)–(18) with the initial condition

$$c(x, t=0) = c_\infty. \quad (23)$$

Since the growth is symmetric with respect to the nucleation plane  $x=0$  we restrict the analysis to the region  $R \leq x < \infty$ . The initial interface velocity  $V_i = V|_{t=0}$  is defined implicitly by  $c_L(V_i) = c_\infty$ .

An approximate solution of this problem is developed along the lines of our previous work [24] devoted to a pure substance. In this approach, termed “the mass balance integral method,” the diffusion equation Eq. (16) is replaced by its zero order moment. Furthermore, one has to assume the spatial dependence of the concentration field in the melt in order to reduce the original problem to the ordinary differential equation. The physics behind the selection of the concentration profile determines the adequacy and the accuracy of the resulting solution.

Integrating Eq. (16) from  $x=R$  to infinity and using Eqs. (17)–(19) one obtains

$$\frac{d}{dt} \int_R^\infty (c - c_\infty) dx = V(c_\infty - kc_L). \quad (24)$$

$$L(t) = \begin{cases} 2\Omega^2(D/V)c^*(1-k^*)(c_L - c_\infty)/c_L(1-k)(c^* - c_\infty), & c_\infty > \max\{kc_L\} \\ (D/V)(c_L - c_\infty)/(1-k)c_L, & c_\infty \leq \max\{kc_L\} \end{cases}. \quad (27)$$

Substituting Eqs. (25) and (26) into the overall mass balance Eq. (24) yields the following equation for the interface velocity:

$$dV/dt = -V^3(c_\infty - kc_L)/U[G - V(dG/dV)]. \quad (28)$$

Here

$$U = \begin{cases} 2\Omega^2 D c^* (1-k^*) (c_\infty - c^* k^*) / (c^* - c_\infty)^2 & c_\infty > \max\{kc_L\} \\ D, & c_\infty \leq \max\{kc_L\} \end{cases} \quad (29)$$

and

$$G = (c_L - c_\infty)^2 / (1-k)c_L. \quad (30)$$

As follows from Eq. (29), for  $k^*c^* < c_\infty \leq \max\{kc_L\}$ , one could use either of the profiles (25) or (26), since  $V(t)$  would be changed only by a constant factor, not affecting the qualitative behavior of the solidification rate.

To summarize: the moving boundary problem, stated by Eqs. (16)–(18), has been reduced to a single ordinary differential equation Eq. (28). The initial velocity  $V_i$  has been defined implicitly by  $c_L(V_i) = c_\infty$ , with  $c_L(V, c^*)$  given by Eq. (7), or Eq. (11). Due to the intrinsic nonlinearity of the above kinetic models Eq. (28) has to be integrated numerically. Yet, this is much less time consuming than the full numerical solution of the original moving boundary problem. The accuracy of the approximate solution is discussed in Sec. VI.

We now prove that in the range of velocities,  $0 < V \leq v_D$ , the growth rate given by Eq. (28) is monotonically decreasing

in time, provided  $c_\infty \geq kc_L$  during the entire process. Indeed, Eq. (30) yields

$$c = c_\infty + (c_L - c_\infty) \frac{\operatorname{erfc}(\Omega\{1 + [x - R(t)]/L(t)\})}{\operatorname{erfc} \Omega}. \quad (25)$$

Here  $\Omega$  is a constant parameter, defined as the real root of Eq. (20). For  $c_\infty \leq \max\{kc_L\}$  the melt concentration is assumed to be represented by the kinetics-type profile

$$c = c_\infty + (c_L - c_\infty) \exp\{-[x - R(t)]/L(t)\}. \quad (26)$$

The assumed profiles involve two time-dependent length scales: the width of the germ, equal to  $2R$ , and the thickness of the diffusion layer in the melt, measured by  $L(t)$ . The above profiles satisfy the initial condition at  $t=0$  and are reducible to the solutions given by Eqs. (19)–(22) when  $L=R$ , or  $L=D/V$  for the diffusion-limited, or the kinetics-limited growth, respectively.

Inserting Eqs. (25) and (26) into the interfacial mass balance Eq. (17) one obtains the following relation between the thickness of the concentration boundary layer and the velocity of the interface:

ing in time, provided  $c_\infty \geq kc_L$  during the entire process. Indeed, Eq. (30) yields

$$\frac{dG}{dV} = \frac{c_L - c_\infty}{c_L(1-k)} \left[ 2 - \frac{c_L - c_\infty}{c_L(1-k)} [1 - (dc_S/dc_L)] \right] \frac{dc_L}{dV}. \quad (31)$$

It is straightforward to show that for both Model A as well as Model B,

$$0 \leq 1 - dc_S/dc_L \leq (1-k) \{1 + [v_0 c^* (1-k^*) / (V + v_D)]\}. \quad (32)$$

As stated in Sec. III in the region  $0 < k < k_D$  of the Baker-Cahn diagram, where the sharp interface models are well defined, the parameters  $c^*$ ,  $k^*$ ,  $v_0$ , and  $v_D$  are restricted by  $c^*(1-k^*)v_0 \leq v_D$ . Therefore

$$0 \leq 1 - dc_S/dc_L \leq 2(1-k) < 2. \quad (33)$$

Using this inequality in Eq. (31) and taking into account that  $(dc_L/dV) < 0$ , and  $c_\infty \geq kc_L$ , it is straightforward to show that  $dG/dV < 0$ . It then follows from Eqs. (28) and (29) that

$$dV/dt < 0, \quad \text{for } 0 < k < k_D, \quad \text{and } c_\infty \geq kc_L. \quad (34)$$

Now let us show that the condition  $c_\infty \geq kc_L$  is satisfied for the germ growth, so that the interface acceleration is negative uniformly in time. Obviously, this condition holds for  $c_\infty \leq \max\{kc_L\}$ . In this case Eq. (28) implies that  $dV/dt \rightarrow 0$  when  $V \rightarrow 0$ . If  $c_\infty \leq \max\{kc_L\}$ , then the interface decelerates at the onset of the solidification process, since  $c_\infty > k(V_i)c_L(V_i)$ . According to Eq. (34) the deceleration of the interface continues as long as  $kc_L < c_\infty$ . The acceleration  $dV/dt$  can change its sign only when the solid composition, at the interface  $c_S = kc_L$  will reach for the first time the value  $c_\infty$ . However, as shown below, for growth with a decelerating interface the state  $kc_L = c_\infty$  serves as the asymptotic attractor when  $t \rightarrow \infty$ . Thus, in this case too  $dV/dt$  is negative during the entire solidification process, and the velocity tends to some constant value  $V_f$  for  $t \rightarrow \infty$ .

When  $c_S = c_S(c_L)$  is a monotonically increasing function the asymptotic state  $V = V_f$  is defined uniquely by Eq. (22), provided  $c_\infty < k^*c^*$ . The nature of the long-time asymptotic attractor for  $c_\infty = k^*c^*$  is discussed in the following section. For nonmonotonic curves  $c_S = c_S(c_L)$  the equation  $kc_L = c_\infty$  admits multiple roots. The infinite time of deceleration from  $V = V_i$  to the asymptotic state  $V = V_f$  singles out as the long-time attractor the root with the largest value of  $V_f$ . This root is located either at the increasing branch of the curve  $c_S = c_S(c_L)$ , or at its maximum.

## V. ASYMPTOTIC SOLUTIONS

Let us first consider the short-time asymptotics. Expanding the interfacial solid and liquid concentrations near their initial values, up to the first order in  $V - V_i$ , one obtains

$$dV/dt \approx \alpha^2/2(V - V_i),$$

$$\alpha^2 = V_i^2 c_\infty^2 [1 - k(V_i)]^2 / U \{ [dc_L/dV]_{V=V_i} \}^2. \quad (35)$$

Integrating this equation yields

$$V \approx V_i - |\alpha| \sqrt{t}. \quad (36)$$

Since  $V(t)$  is decreasing in time the minus sign is selected in Eq. (36) According to Eq. (27), at short times the width of the diffusion layer  $L(t)$  increases as  $\sqrt{t}$ , whereas the size of the germ  $R(t)$  is growing as  $t$ . Notice that the short-time asymptotics of  $L(t)$  and  $R(t)$  is similar to that found for a pure substance [24].

Let us now consider in detail the long-time asymptotic solutions of Eq. (28). We begin with the asymptotic states, for which the interface velocity tends to zero. Expanding the liquid and the solid concentrations at the interface near their equilibrium values one obtains

$$c_L = c^* + a_1 V + a_2 V^2 + 0(V^3), \quad (37a)$$

$$c_S = k^* c^* + b_1 V + b_2 V^2 + 0(V^3), \quad (37b)$$

where

$$a_1 = (dc_L/dV)_{V=0} < 0, \quad a_2 = \frac{1}{2}(d^2c_L/dV^2)_{V=0}, \quad (38)$$

$$b_1 = (dc_S/dV)_{V=0}, \quad b_2 = \frac{1}{2}(d^2c_S/dV^2)_{V=0}. \quad (39)$$

Consequently,

$$\frac{dV}{dt} = - \frac{V^3 c^* (1 - k^*) (c_\infty - k^* c^* - b_1 V - b_2 V^2)}{U(c^* - c_\infty)^2 [1 + O(V^2)]}. \quad (40)$$

The solutions of Eq. (40) can be classified as follows: (1)  $c_\infty > k^* c^*$ . ( $St < 1$ .) In this case the long-time solution is diffusion-dominated and the interface velocity decays in time as

$$V(t) = \frac{\Omega \sqrt{D}}{\sqrt{t}} \left[ 1 + \frac{b_1 \Omega \sqrt{D}}{(c_\infty - k^* c^*) \sqrt{t}} + O(t^{-1}) \right]. \quad (41)$$

Consequently, both  $L(t)$  and  $R(t)$  increase in time as  $\sqrt{t}$ . (2)  $c_\infty = k^* c^*$ . ( $St = 1$ .) As follows from Eq. (40)  $b_1$  is either negative, or equal to zero. In the latter case the coefficient  $b_2$  has to be negative. The solution of Eq. (40) is then given by

$$V(t) = \{ [-Dc^*(1 - k^*)] / 3b_1 t \}^{1/3} [1 + O(t^{-1/3})], \quad b_1 < 0, \quad (42)$$

$$V(t) = \{ [-Dc^*(1 - k^*)] / 4b_2 t \}^{1/4} [1 + O(t^{-1/4})], \quad b_1 = 0, \quad b_2 < 0. \quad (43)$$

The ratio of the width of the diffusional boundary layer to the germ thickness  $L(t)/R(t)$  decreases as  $1/t^{1/3}$  for  $b_1 < 0$ , and as  $1/\sqrt{t}$  for  $b_1 = 0$ .

Equations (41)–(43) demonstrate that decay of the transients is correlated with the asymptotic solidification rates. The maximal duration of transient corresponds to  $V \sim t^{-1/4}$ .

Let us now consider the approach to the long-time asymptotic attractors with the constant velocity of the interface  $V_f > 0$ . These attractors are defined by Eqs. (21) and (22) with  $k_f = k(V_f)$ ,  $c_{Sf} = c_\infty$ , and  $c_{Lf} = c_\infty/k_f$ . In the vicinity of  $c_{Lf}$  and  $c_{Sf}$  one can expand  $c_S$  and  $c_L$  in power series:

$$c_L = c_{Lf} + \alpha_1 (V - V_f) + \alpha_2 (V - V_f)^2 + \dots, \quad (44)$$

$$c_S = c_\infty + \beta_1 (V - V_f) + \beta_2 (V - V_f)^2 + \dots. \quad (45)$$

Here

$$\alpha_1 = (dc_L/dV)_{V=V_f} < 0, \quad \alpha_2 = \frac{1}{2}(d^2c_L/dV^2)_{V=V_f}, \quad (46)$$

$$\beta_1 = (dc_S/dV)_{V=V_f}, \quad \beta_2 = \frac{1}{2}(d^2c_S/dV^2)_{V=V_f}. \quad (47)$$

For  $\beta_1 < 0$ , Eqs. (28)–(30) yield in the lowest order

$$dV/dt \approx \beta_1 V^3 (V - V_f) / D [c_{Lf} (1 - k_f) - V_f (\alpha_1 + \beta_1)]. \quad (48)$$

Since  $dc_L/dV < 0$ , the coefficient  $\alpha_1$  is always negative. The solution of Eq. (48) reads

$$V \approx V_f + A \exp(-t/t_r). \quad (49)$$

TABLE I. Input-output data for Model A.

St	$c_\infty = c_{Li}$ at. % Cu	$c_{Si}$ at. % Cu	$V_i/V_D$	$c_{Lf}$ at. % Cu	$c_{Sf}$ at. Cu %	$V_f/V_D$
0.94	0.095	0.046	0.659	0.264	0.095	0.344
0.92	0.102	0.049	0.645	0.348	0.102	0.216
0.50	0.285	0.098	0.314	0.500	0.070	0

Here  $A$  is some constant and  $t_r$  is the relaxation time, given by

$$t_r = D[c_{Lf}(1 - k_f) - V_f(\alpha_1 + \beta_1)]/|\beta_1|V_f^3. \quad (50)$$

If  $\beta_1 = 0$ , then  $\beta_2 < 0$ , and the constant velocity asymptotic attractor is represented by the maximum of the curve  $c_S = c_S(c_L)$ . In this case instead of the exponential decay,  $V(t)$  decreases as  $1/t$

$$V \approx V_f + (t_r'/t), \quad (51)$$

where

$$t_r' = D[c_{Lf}(1 - k_f) - V_f\alpha_1]/|\beta_2|V_f^3. \quad (52)$$

## VI. NUMERICAL RESULTS

The approximate solution developed within the mass balance integral method has been applied to the planar isothermal growth of a solid germ in a dilute Al-Cu alloy. Physical constants for this alloy have been adopted from Ref. [37]. The melting point of pure Al is 933 K. The equilibrium phase diagram is defined by  $k^* = 0.14$ ,  $m^* = 6.07$  K/at. % Cu. The kinetic parameters are given by  $v_D = 4.9$  m/s,  $v_0 = 1000$  m/s, and  $D = 4.9 \times 10^{-9}$  m<sup>2</sup>/s. The equilibrium melt concentration at the interface,  $c^* = 0.5$  at. % Cu, has been selected. For this value of  $c^*$  the version A of the continuous growth model yields a nonmonotonic curve  $c_S = c_S(c_L)$ . Its maximum,  $c_{SQ} = 0.102$  at. % Cu, is located at  $c_{LQ} = 0.353$  at. % Cu. On the other hand, for the above value of  $c^*$  the curve  $c_S = c_S(c_L)$ , corresponding to the version B of the continuous growth model, is monotonically increasing from zero to  $k^*c^*$ . The curves corresponding to the above models are depicted in Fig. 1.

For version A of the continuous growth model three cases have been considered. They are presented in Table I and in Fig. 4. The first case corresponds to the initial melt composition  $c_{Li} = c_\infty$  that yields for  $t \rightarrow \infty$  the constant velocity asymptotic attractor, located on the growing branch of the curve  $c_S = c_S(c_L)$ . This asymptotic attractor exists at  $St = 0.94$ , i.e., below the critical value  $St = 1$ , that separates the kinetics-limited growth from the diffusion-limited regime in the models without the solute trapping effects. In this case the transient is short lived, corresponding to the exponential relaxation to the asymptotic attractor. The second case with  $St = 0.92$  is at the crossover between the kinetics-limited and the diffusion-limited long-time asymptotic states. It corresponds to the trajectory, which tends to the maximum of  $c_S = c_S(c_L)$  as  $t \rightarrow \infty$ . The solution for this case involves the long-lived transient that tends asymptotically to the constant velocity attractor. Finally, the third case with  $St = 0.5$  describes evolution towards the diffusion-controlled growth.

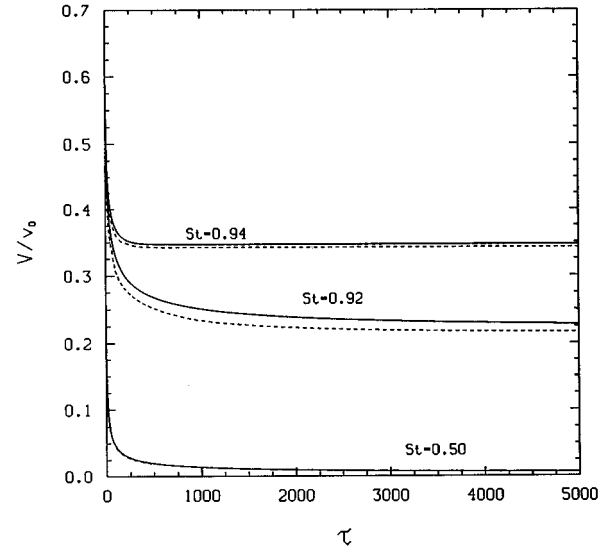


FIG. 4. Dimensionless velocity,  $V/v_D$ , as a function of dimensionless time,  $\tau = t v_D^2/D$ , for Model A. Al-Cu alloy at  $c^* = 0.5$  at. % Cu. Solid lines—the approximate solution, Eqs. (23), (28)–(30). Dashed lines—the numerical solution of the original moving boundary problem, Eqs. (16)–(18), (23).

This case too demonstrates a typical solute trapping effect: the solute concentration in the solid is approaching its equilibrium value *from above* when the solidification process evolves towards the diffusion-limited regime. The growth velocity drops by two orders of magnitude from its initial value during the time interval of the order  $10^{-6}$  s.

The transient solidification has also been inspected for Model B. As mentioned above for  $c^* = 0.5$  this model does not exhibit the solute trapping effects: the kinetics-limited growth at long times is allowed only for  $St > 1$ , whereas the diffusion-controlled growth at long times corresponds to  $St < 1$ . The input-output data for two representative cases  $St = 1.02$  and  $St = 0.75$  are given in Table II and the velocity relaxation curves are depicted in Fig. 5. For  $St = 1.02$  the initial velocity is the same as for the case  $St = 0.94$  for Model A. As in Model A there is exponential relaxation of the velocity to its asymptotic value  $V_f = 0.320 v_D$ . It is lower than  $0.344 v_D$ , corresponding to Model A. For the second case,  $St = 0.75$ , the initial velocity is the same as that for the  $St = 0.5$  case of Model A. The relaxation to the diffusional regime at long times is accompanied now by a monotonic increase of the solute concentration in the solid.

In order to validate the approximate solution, derived using the mass balance method, we have developed the numerical solution of the original moving boundary problem as stated by Eqs. (16)–(18). The explicit finite difference scheme with the fixed grid has been adopted for this purpose. It is based on the algorithm originally designed for the clas-

TABLE II. Input-output data for Model B.

St	$c_\infty = c_{Li}$ at. % Cu	$c_{Si}$ at. % Cu	$V_i/V_D$	$c_{Lf}$ at. % Cu	$c_{Sf}$ at. Cu %	$V_f/V_D$
1.02	0.060	0.029	0.659	0.174	0.060	0.320
0.75	0.177	0.061	0.314	0.500	0.070	0

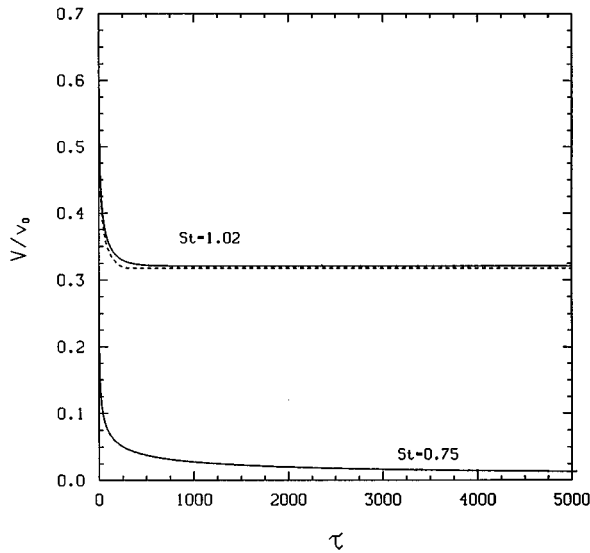


FIG. 5. Dimensionless velocity,  $V/v_D$ , as a function of dimensionless time,  $\tau = tv_D^2/D$ , for Model B. Al-Cu alloy at  $c^* = 0.5$  at. % Cu. Solid lines—the approximate solution, Eqs. (23), (28)–(30). Dashed lines—the numerical solution of the original moving boundary problem, Eqs. (16)–(18), (23).

sical Stefan problems with constant temperature or concentration at the moving boundary [40]. This scheme uses the Taylor series expansions which result in a polynomial fit for forward interpolation of the concentration or temperature fields at the nodal points, located in the vicinity of the interface. This scheme successfully handles the nonlinearities of the Stefan problem and yields accurate and stable solutions with relatively low CPU time in a wide range of the Stefan numbers. The latter numerical scheme has been extended in order to incorporate the out-of-equilibrium conditions at the interface. The concentration gradient at the interface has been evaluated at each time step in order to calculate the interface velocity via the kinetic liquidus equation. The spatial domain has been divided into two subdomains, estimated using the approximate solution of the problem. The inner domain, located in the vicinity of the interface had a high resolution grid, whereas the outer domain had a grid with a lower resolution. The solutions for each domain have been matched at each time step. The time step has been selected according to the stability criterion of the explicit finite difference scheme in the high resolution domain, and the actual step used in the calculations has been smaller than the above one by an order of magnitude. This numerical scheme has been validated by comparison with the numerical solution of the moving boundary problem with linear interfacial kinetics, as given in [24]. The program has been run on the Spark 10 Sun computer. The running time, required to approach the long-time asymptotic states, varied from 5 to 50 h, for solutions with short-lived and the long-lived transients, respectively.

The functions  $V(t)$ , calculated within the numerical solution of the original moving boundary problem for the specific cases given in Tables I and II, are represented by the dashed lines in Figs. 4 and 5. These curves explicitly demonstrate that the approximate solution, obtained in the framework of the mass balance integral method, reproduces with a reason-

able accuracy the main features of the numerical solution of the full problem.

## VII. CONCLUDING REMARKS

In the present paper we studied the solute trapping effects in transient isothermal solidification of the dilute binary alloys. The planar growth of a germ, nucleated in a melt at a uniform concentration, below its equilibrium value, has been considered. Assuming the boundary layer-type melt concentration profiles and replacing the diffusion equation by its zero order moment, the original moving boundary problem has been reduced to an initial value problem for a single ordinary differential equation for the interface velocity. Evolution of the germ has been represented on the Baker-Cahn diagram by trajectory along the curve  $c_S = c_S(c_L)$ , corresponding to some specific kinetics model.

This approximate solution has been integrated numerically for the dilute Al-Cu alloy. The results are in agreement with the numerical solution of the original moving boundary problem.

Within the approximate solution the main evolution characteristics of the germ growth are reduced to the width of the solid germ  $R(t)$  the thickness of the boundary layer in the melt  $L(t)$  and the interfacial concentrations of the liquid  $c_L$  and the solid  $c_S$ . These quantities are uniquely determined by the solidification rate  $V(t)$  the kinetics model, the equilibrium phase diagram ( $c^*(T), k^*$ ), and the initial concentration of the melt  $c_\infty$ .

For both versions of the continuous growth model we have shown that the growth rate of the germ is monotonically decreasing in time. Simultaneously the rejection of the impurities from the solid raises the melt composition at the interface. The time dependence of the solid composition  $c_S$  is more complicated. It reflects the specifics of the interfacial kinetics model and depends on the initial melt composition  $c_\infty$  as well as on its equilibrium composition  $c^*$  at some prescribed temperature.

When  $c^*$  is below some model-dependent threshold concentration  $c_{cr}^*$  the curves  $c_S = c_S(c_L)$  are monotonically increasing, so that the solid concentration at the interface  $c_S$  is increasing in the course of the germ growth. This behavior is similar to that found in models without the solute trapping effects. For  $c_\infty < k^*c^*$  ( $St > 1$ ) the long-time asymptotic state is the plane wave traveling with a constant velocity. For  $c_\infty > k^*c^*$  ( $St < 1$ ) the long-time regime is diffusion dominated, and for  $c_\infty = k^*c^*$  ( $St = 1$ ) the solidification rate tends to zero as  $V \sim 1/t^{1/3}$ . The last case is characterized by a long-lived transient. The solute trapping effects become significant for  $c^*$  equal or greater than the threshold concentration  $c_{cr}^*$ . In this case the curves  $c_S = c_S(c_L)$  are no longer monotonic.

For version A of the continuous growth model at  $c^* = c_{cr}^*$  and  $c_\infty = k^*c^*$  ( $St = 1$ ) the long-time behavior of the interface velocity is given by  $V \sim 1/t^{1/4}$ , rather than  $1/t^{1/3}$ . For  $c^* > c_{cr}^*$  the curves  $c_S = c_S(c_L)$  have one maximum at  $c_L = c_{LQ} < c^*$ . If  $c_\infty \leq c_{SQ} = k_Q c_{LQ}$  ( $St \geq St_Q$ ) the evolution of the germ is represented by the trajectory along the increasing branch of the curve  $c_S = c_S(c_L)$ . The long-time attractors are again waves, propagating with some constant velocity. Due to the solute trapping effects these attractors are located not

only in the region  $St > 1$ , but also in the interval  $St_Q < St < 1$ , forbidden for the kinetics models without solute trapping. The duration of the transients increases when  $St \rightarrow St_Q$ . As long as  $St > St_Q$  the transients decay exponentially in time. For  $St = St_Q$ , i.e., at the crossover between the diffusion-limited and the kinetics-limited long-time regimes, the transients decay as  $1/t$ . For  $c_\infty > c_{SQ} = k_Q c_{LQ}$  ( $St < St_Q$ ) the long-time regime is diffusion dominated. Since  $c_S > k^* c^*$ , this diffusion-controlled growth differs from that observed in the models without solute trapping by a decrease (instead of an increase) of the solid concentration at the interface during germ growth. Furthermore, if the initial concentration in the melt  $c_{Li}$  is in the interval  $(c_{SQ}, c_{LQ})$ , then the corresponding trajectory on the Baker-Cahn diagram is nonmonotonic: the initial increase of  $c_S$  towards its maximal value  $c_{SQ}$  is followed by the subsequent decrease towards  $k^* c^*$ .

For version B of the continuous growth model the curve  $c_S = c_S(c_L)$  has a saddle point at  $c^* = c_{cr}^*$ . When  $c^*$  is above  $c_{cr}^*$ , the saddle point splits into the maximum (at  $c_L = c_{LQ1}$ ) and the minimum (at  $c_L = c_{LQ2} > c_{LQ1}$ ). When  $c_\infty < \max\{c_{SQ1}, k^* c^*\}$  the growth rate tends exponentially to some constant value  $V_f > 0$ . These constant velocity traveling wave-type long-time asymptotic attractors are located on the increasing branch of  $c_S = c_S(c_L)$ . If at the maximum of the latter curve  $c_{SQ1} \geq k^* c^*$  then for  $c_\infty = c_{SQ1}$ , the long-time attractor is also the constant velocity traveling wave. However, in this case the deceleration of the interface follows  $1/t$  law. When  $c_{SQ1} < k^* c^*$ , there are also constant velocity asymptotic attractors for  $c_{SQ1} \leq c_\infty < k^* c^*$ . At  $c_\infty = k^* c^*$  the growth rate tends to zero as  $1/t^{1/3}$ , just as for the kinetics models without the solute trapping. For  $c_\infty > \max\{c_{SQ1}, k^* c^*\}$  the long-time regime is diffusion dominated. In this case for sufficiently large times  $c_S$  is always smaller than its equilibrium value  $k^* c^*$  just like in the models without the solute trapping effects.

Since the threshold concentration is a model-dependent quantity, the alternative versions of the continuous growth model might yield different long-time asymptotic states for identical initial conditions. In particular, for  $St = 1$  Model A might yield at long times the traveling wave propagating with a constant velocity, whereas Model B might yield in this case  $V \sim 1/t^{1/3}$ .

Before concluding we would like to comment on the transient thermal effects disregarded in the above analysis. Rapid solidification of alloys implies fast removal of the latent heat of fusion. In general, part of this heat is absorbed by the alloy itself, whereas the rest of it is removed by some external heat sinks. According to Misbah, Muller-Krumbhaar, and Temkin [38] the growth into the undercooled melt can be treated as isothermal if

$$\varepsilon = (T_i - T_\infty) / (T_0 - m^* c_\infty - T_\infty) \ll 1. \quad (53)$$

Here  $T_i$  is the interface temperature, and  $T_\infty$  is the temperature far from the interface. Let us first consider the release of the latent heat into the melt, by applying Eq. (53) to two prototypical problems with equilibrium conditions at the interface. The first problem is addressing the planar growth into undercooled melt. Its solution is obtained by combining the similarity solution Eqs. (19) and (20) with the same type solution for the temperature. The second problem considers a

slow radial growth into an undercooled melt as given in [10]. It can be shown that for these problems

$$\varepsilon \approx (L/C) Le^n / m^* c^* (1 - k^*). \quad (54)$$

Here  $L$  is the latent heat,  $C$  is the specific heat of the melt, and  $n$  is the parameter, equal to  $1/2$  for the planar case, and to unity for the spherical growth. For the dilute Al-Cu alloy,  $L/C$  is about 300,  $Le \approx 10^{-4}$ , and  $\varepsilon \leq 0.1$  would require  $c^* \geq 5$  at. % Cu. On the other hand, in order to preserve the validity of the sharp interface model ( $V < v_D$ ) for the entire range of  $c_\infty$  we had to restrict the analysis to the substantially lower values of  $c^*$ . Therefore in this range of parameters the release of the latent heat of fusion into melt is expected to play an important role for the planar setup not only for large velocities but even for the diffusion-limited growth.

For the spherically symmetric case Eq. (54) suggests that the thermal effects would be reduced by two orders of magnitude ( $\sqrt{Le}$ ). Within this context the solutions developed in our paper, which mimic the radial growth of a germ, might be relevant when the curvature effects are small, while the interfacial kinetics still affects the solidification rate. Notice, that this interpretation is meaningful only for sufficiently small interface velocities, i.e., for processes that tend towards the diffusion-limited long-time regime. Analysis of the radial growth for the large velocities faces, however, an unsolved problem associated with the generalization of the Gibbs-Thompson effect to the far-from-equilibrium conditions [37].

Let us now consider the planar setup with some appropriate external heat sinks. In this case the solutions developed above are adequate, provided the latent heat released at the interface is rapidly conducted away. For a crystalline alloy growing on a substrate this can be achieved, at least in principle, by removal of the latent heat into a solid. Obviously, for this purpose one would have to determine the appropriate cooling strategy. In order to exemplify this approach let us consider the diffusion-limited growth given by Eqs. (19) and (20). This solution can be matched with the solution of the thermal Stefan problem in the solid, with the fixed boundary maintained at some constant temperature  $T_w$  [1]. (The latter solution also yields the parabolic law for the interface advance). It can be shown that  $T_w$  is related to  $T_\infty$  by

$$T_\infty - T_w = 2\Omega^2 (L/C_s) (D/D_{Ts}). \quad (55)$$

Here the subscript ‘‘s’’ stands for solid. For  $St = 0.5$ , the temperature difference  $T_\infty - T_w$  is of the order 0.01 K. The constant temperature control applies only at long times, whereas the transient regime requires a time-dependent cooling strategy. As shown in Sec. VI for  $St = 0.5$  the germ emerges with the initial interface velocity of about 1.5 m/s. Its velocity drops by a factor of 100, approaching the diffusion-limited regime during the relaxation time of the order of  $10^{-6}$  s. The cooling rates needed for transitions to the constant velocity attractors are higher. In order to maintain the constant velocity solutions the temperature at the fixed wall of the solid has to decrease exponentially in time. In the general case, in order to preserve the isothermal conditions in the melt for the transient growth one has to match the solution of the isothermal solidification problem in the liquid with the solution of the appropriate inverse thermal Stefan problem in the solid. The mathematical correctness of

the latter problems with prescribed temperature and velocity of the interface is well established and the numerical solutions of such problems are discussed in [41].

We realize that it would be rather difficult to maintain the isothermal conditions in the melt. In spite of this, similar to the  $Le=0$  limit, explored in the studies of directional solidification, the results of the present paper represent a first step and the reference point for a more comprehensive analysis of rapid solidification into an undercooled melt. The solutions developed in the paper serve as a sufficiently simple and accurate theoretical tool to inspect several important aspects of the continuous growth models versus the models ignoring the solute trapping effect. These solutions also demonstrate

that the alternative versions of the continuous growth models yield quite different results even for relatively small growth rates. The problem of the nonisothermal growth of a solid germ, which is a natural extension of the present work, is now under study.

#### ACKNOWLEDGMENTS

We express our gratitude to C. Caroli, B. Caroli, M. Glicksman, and J. W. Cahn for stimulating discussions and encouragement at the early stage of this work. We appreciate the suggestions of B. Zaltzman concerning the numerical solution of the original moving boundary problem.

- 
- [1] H. S. Carslaw and J. C. Jaeger, *Conduction of Heat in Solids* (Oxford University Press, Oxford, 1959).
- [2] C. Zener, *J. Appl. Phys.* **20**, 950 (1949).
- [3] W. W. Mullins and R. F. Sekerka, *J. Appl. Phys.* **35**, 444 (1964).
- [4] M. E. Glicksman and R. J. Shaefer, *J. Cryst. Growth* **1**, 297 (1967).
- [5] R. J. Shaefer and M. E. Glicksman, *J. Cryst. Growth* **5**, 44 (1969).
- [6] J. C. Baker and W. J. Cahn, *Acta Metall.* **17**, 575 (1969).
- [7] J. C. Baker and W. J. Cahn, in *Solidification* (American Society for Metals, Metals Park, OH, 1971).
- [8] J. S. Langer, *Rev. Mod. Phys.* **52**, 1 (1980).
- [9] R. F. Sekerka, in *Interfacial Aspects of Phase Transformations, Proceedings of the NATO Advanced Study Institute, Erice, 1981*, edited by B. Mutaftschiev (Reidel, Dordrecht, 1982).
- [10] B. Caroli, C. Caroli, and B. Roulet, in *Solids Far From Equilibrium*, edited by C. Godreche (Cambridge University Press, Cambridge, 1992).
- [11] Ch. Charach and I. Rubinstein, *J. Appl. Phys.* **71**, 1128 (1992).
- [12] W. J. Boettinger and S. R. Coriell, in *Science and Technology of the Undercooled Melt*, edited by P. R. Sahm, H. Jones, and C. M. Adam (NASA, Greenbelt, MD, 1986).
- [13] W. J. Boettinger and J. H. Perepezko, in *Rapidly Solidified Alloys*, edited by H. L. Liebermann (Dekker, New York, 1993), and references therein.
- [14] K. A. Jackson, *Can. J. Phys.* **36**, 683 (1958).
- [15] G. M. Kudinov, D. E. Temkin, and B. Y. Lyubov, *Phys. Met. Metall.* **46**, 73 (1978).
- [16] B. Caroli, C. Caroli, and B. Roulet, *Acta Metall.* **34**, 1867 (1986).
- [17] M. J. Aziz, *J. Appl. Phys.* **53**, 1158 (1982).
- [18] M. A. Aziz and T. Kaplan, *Acta Metall.* **36**, 2335 (1988).
- [19] M. J. Aziz and W. J. Boettinger, *Acta Metall.* **42**, 527 (1994).
- [20] P. M. Smith and M. J. Aziz, *Acta Metall.* **42**, 3515 (1994).
- [21] A. Umantsev, *Kristallografiya* **30**, 153 (1985) [*Sov. Phys. Crystallogr.* **30**, 87 (1985)].
- [22] J. N. Dewynne, S. D. Howison, J. R. Ockendon, and Weiqing Xie, *J. Aust. Math. Soc. B* **31**, 81 (1989).
- [23] Ch. Charach and B. Zaltzman, *Phys. Rev. E* **47**, 1230 (1993).
- [24] Ch. Charach and B. Zaltzman, *Phys. Rev. E* **49**, 4322 (1994).
- [25] H. Lowen, J. Bechhoefer, and L. Tuckerman, *Phys. Rev. A* **45**, 2399 (1992).
- [26] M. Marder, *Phys. Rev. A* **45**, R2158 (1992).
- [27] J. B. Collins and H. Levine, *Phys. Rev. B* **31**, 6119 (1985).
- [28] J. S. Langer, in *Directions in Condensed Matter Physics*, edited by G. Grinstein and G. Mazenko (World Scientific, Singapore, 1986).
- [29] P. C. Fife, *Dynamics of Internal Layers and Diffuse Interfaces* (SIAM, Philadelphia, 1988).
- [30] O. Penrose and P. C. Fife, *Physica D* **69**, 107 (1993).
- [31] S. L. Wang, R. F. Sekerka, A. A. Wheeler, B. T. Murray, S. R. Coriell, R. J. Braun, and G. B. McFadden, *Physica D* **69**, 189 (1993).
- [32] A. A. Wheeler, W. J. Boettinger, and G. B. McFadden, *Phys. Rev. E* **47**, 1893 (1993).
- [33] J. Frenkel, *Kinetic Theory of Liquids* (Dover, New York, 1955).
- [34] D. Turnbull, *Solid State Phys.* **3**, 225 (1956).
- [35] G. Merchant and S. H. Davis, *Acta Metall. Mater.* **40**, 2683 (1990).
- [36] A. Karma and A. Sarkissian, *Phys. Rev. E* **47**, 513 (1993).
- [37] D. A. Huntley and S. H. Davis, *Acta Metall. Mater.* **41**, 2025 (1993).
- [38] C. Misbah, H. Muller-Krumbhaar, and D. E. Temkin, *J. Phys. 1 (France)* **1**, 585 (1991).
- [39] Ch. Charach (unpublished).
- [40] M. Sokolov and Y. Keizman, *Int. J. Num. Meth. Heat Fluid Flow* **2**, 215 (1992).
- [41] K. H. Hoffman and M. Niezgodzka, in *Free and Moving Boundary Problems*, Research Notes in Mathematics Vol. 79, edited by A. Fasano and M. Primicerio (Pitman, Boston, 1983).